DOI: 10.61782/fa.2023.0814

forum acusticum 2023

EXPERIMENTAL STUDY OF SURFACE NOISE MITIGATION FOR PROPELLER IN BOUNDARY LAYER INGESTION CONFIGURATION

Leandro A. Castelucci[1*] **Cornelis H. Venner**[1] **Ysbrand H. Wijnant**[1]
[1] Department of Thermal Fluid Engineering, University of Twente, Netherlands

ABSTRACT

Noise mitigation is critical in the conceptual designs of aircraft. The evolving requirements for noise reduction and the urbanization of aircraft are some reasons why reducing noise is crucial when designing new concepts. Those novel configurations can include complex propulsion-air frame interactions, such as boundary layer ingestion. While research focuses on shrouded solutions, airframe noise mitigation optimization presents a solution for designs that cannot apply shrouding. This paper shows an experimental analysis of surface noise mitigation underneath a propeller under boundary layer ingestion. The propeller is set on the bottom wall of the wind tunnel to generate the boundary layer ingestion. Tripping devices are used to change the boundary layer thicknesses of the flow impinging on the propeller. The noise reduction surfaces are positioned underneath the propeller through a slot on the flat plate. The surface analyzed is a known frequency absorber (quarter-wave resonator) separated from the flow by a Kevlar panel. Two microphone arrays capture the noise coming from the propeller. The results show that the mitigation strategy reduces noise close to the frequencies of interest, but increases the tonal levels of the propeller due to the resonance with the quarter-wave resonators.

Keywords: *propeller noise, passive noise mitigation, boundary layer ingestion, wind tunnel*

**Corresponding author*: *l.a.castelucci@utwente.nl.*

1. INTRODUCTION

The urbanization of aircraft and the necessity of complying with increasingly strict regulations make noise one of the most important themes in modern aviation design [1,2]. For complex propulsive-airframe interactions, when the flow around the airframe and entering the propulsive system are coupled, the effects of this coupling on generated noise are not obvious [3]. Also, on the design level, propellers reached a peak in optimization. [4]. Nowadays shrouding is one of the most common solutions for noise mitigation [5]. However, an alternative solution is needed when shrouding is not an option, such as surfaces close to the propulsive system with noise absorption techniques. This results in the absorption of the propeller noise irradiated to the far field. This research is a baseline study of the effects of passive noise control surfaces on the surface underneath a propeller with boundary layer ingestion. The experimental analysis aims to show the possibility of reducing noise by using a quarter-wave resonator structure and analyzing its directivity.

2. METHODOLOGY

2.1 Low reduced frequency model

The noise absorbtion elements are designed using the Low reduced frequency model [6] for coupled prisms. Starting from Navier-Stokes equations, the energy equation and ideal gas equations of state, Helmholtz equation is obtained considering viscosity and thermal effects (Equations 1 and 2).

$$p(x_t) = \hat{p}_A e^{\Gamma k x_t} + \hat{p}_B e^{-\Gamma k x_t} \tag{1}$$

$$u(x_t) = -\frac{G}{\rho_0 c_0}(-\hat{p}_A e^{\Gamma k x_t} + \hat{p}_B e^{\Gamma k x_t}) \quad (2)$$

Where $p(x_t)$ is a sound field consisting of plane waves moving inside the prismatic tube along the longitudinal direction x_t of the tube. The wave propagation coefficient Γ is a complex number of which the imaginary part is related with the phase velocity, and the real part is related with the attenuation. This value is related to the geometry of the tube. The coefficient G is related to the cross-section type.

Viscous and thermal considerations are added using specific dimensional parameters. The formulation below uses the following nomenclature: ω is the angular frequency, c_0 is the reference sound speed, μ is the dynamic viscosity, C_P and C_V are the specific heats for ideal gas. The following formulation analyses a single tube of radius r and length L.

The shear wave number $s = r\sqrt{\rho_0 \omega/\mu}$ is the ratio between inertial and viscous forces. This non dimensional value determines the velocity profile inside the tube. Low values of s indicates viscosity dominating whereas high values indicate that inertial forces are dominating the velocity profile. The reduced frequency $k_r = r\omega/c_0$ is the ratio between the length of the tube and the acoustic wavelength. The low reduced frequency model is valid for a specific range of k_r and s. The square root of the Prandtl number $\sigma = \sqrt{\mu C_P/\lambda}$ and the ratio of specific heats $\gamma = C_P/C_V$ are constant for ideal gases. The expression for acoustic impedance is:

$$\zeta(x_t) = \frac{-G}{\rho_0 c_0}\frac{p(x_t)}{u(x_t)} \quad (3)$$

Using Equations 1 and 2, the acoustic impedance can be written in the following form:

$$\zeta(L) = \frac{\sinh(\Gamma k L)}{p(0)/p(1) - \cosh(\Gamma k L)} \quad (4)$$

where $p(1)/p(0) = 1/\cosh(\Gamma k L)$. In that way, the impedance is related with the tube length L.

The ratio between the reflected and incident wave $R(x_t)$ is a suitable way to show sound absorption and reflection. The reflection coefficient R is written as

$$R(x_t) = \frac{\zeta(x_t) - 1}{\zeta(x_t) + 1} \quad (5)$$

Finally, the coefficient of absorption expresses the dissipation of incident energy by the surface:

$$\alpha = 1 - |R|^2 \quad (6)$$

This methodology can be applied to a collection of tubes, considering them as coupled prisms. This is done using the concept of surface porosity defined as follows:

$$\Omega = N A_{tube}/A_{wall} \quad (7)$$

Where N is the number of tubes of a given cross-sectional area, on a wall surface with area A_{wall} and A_{tube} is the cross-section of the tubes. The scaled impedance of the wall can be related to the individual porosity contribution of each tube with Equation 8. It uses the collection of tubes i that represents a specific impedance Ω_i.

$$\zeta_{wall} = \frac{1}{\sum \frac{\Omega_i}{\zeta_i}} \quad (8)$$

where ζ_i is the impedance of each tube of length L_i, obtained with Equation 4. The absorption coefficient of the whole piece is obtained using Equation 6, with the reflection coefficient R_{wall} calculated with the wall impedance of Equation 8.

3. EXPERIMENTAL SETUP

The experiments are executed in the University of Twente acoustic wind tunnel [7]. The facility consists of a $6 \times 6 \times 4\ m^3$ anechoic chamber in which the test section of the wind tunnel is installed. The chamber is ISO 3745 norm commissioned for a cut-off frequency of 160 Hz. The wind tunnel has a $0.9 \times 0.7\ m^2$ rectangular test section, with maximum flow speed of $60\ m/s$ and a turbulence intensity below $0.1\ \%$.

This experimental setup uses a 2-bladed Meijzlik $12" \times 18"$ propeller. Its geometry is provided by the project *SilentProp* [8]. The propeller is immersed in the boundary layer of the wind tunnel bottom wall. The boundary layer impinging on the propeller is controlled by 60° zigzag tripping devices positioned $3620\ m$ upstream of the propeller plane to ensure a fully developed boundary layer [9]. Figure 1 shows a schematic of the configuration.

The tripping device height controls the boundary layer thickness. Trip 0 is the flat plate only. Trip 1 and Trip 2 have $8\ mm$ and $12\ mm$ trip heights, respectively. Table 1 lists conditions at the propeller plane of the resulting boundary layer for each trip.

Considering x as the distance between the tripping device and the propeller plane, ν the kinematic viscosity of

Table 1. Boundary layer characteristics at the propeller plane for each tripping device.

Trip	$\delta(mm)$	H	Re_x	Re_θ
Trip 0	56.5	1.32	7.28×10^6	18550
Trip 1	102.5	1.27	7.29×10^6	22370
Trip 2	139.8	1.24	6.82×10^6	33920

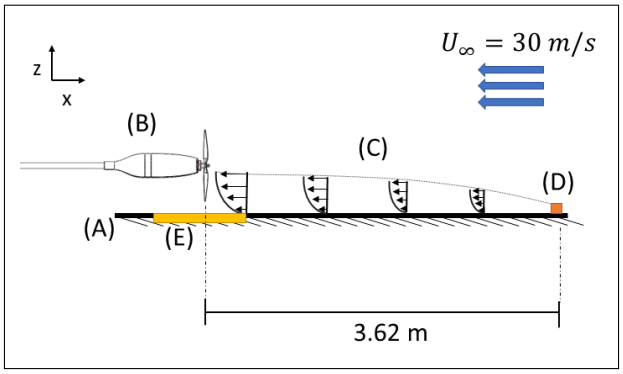

Figure 1. Propeller position and tripping schematics. (A) Flat plate; (B) propulsive system; (C) turbulent boundary layer; (D) tripping device; (E) Quarter wave resonator elements.

air, and U_∞ the flow speed we have: the boundary layer thickness δ is the position where $u(y) = 0.99 \times U_\infty$; H is the form factor. The Reynolds number of the distance of development x is $Re_x = x \times U_\infty/\nu$; and finally the Reynolds number of the momentum thickness θ is $Re_\theta = \theta \times U_\infty/\nu$.

Two microphone arrays (Figures 2 and 3) are used to acquire acoustic data. A polar array with 17 microphones is positioned perpendicular to the propeller plane above the propeller disk, with the microphones facing the flat plate underneath the propeller (Figure 2). A linear array with ten microphones is positioned by the side of the wind tunnel, perpendicular to the propeller plane. Previous studies by Castelucci et al. [10] and Guerin et al. [11] showed that the arrays behave differently due to the noise reflections on the flat plate. The polar array has an increased sound level due to the direct reflections from the flat plate.

The microphones used are GRAS 40PH free-field microphones for both arcs, connected to a *PXIe-4499* Sound

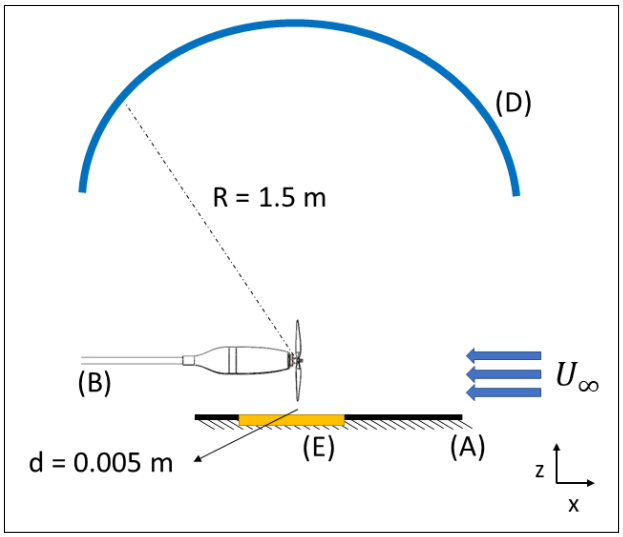

Figure 2. Polar array (side view). An arc of microphones is positioned at a radius R = 1.5m from the propeller center. (A) Flat Plate; (B) Propulsive system; (D) Polar array of microphones; (E) Quarter wave resonator elements

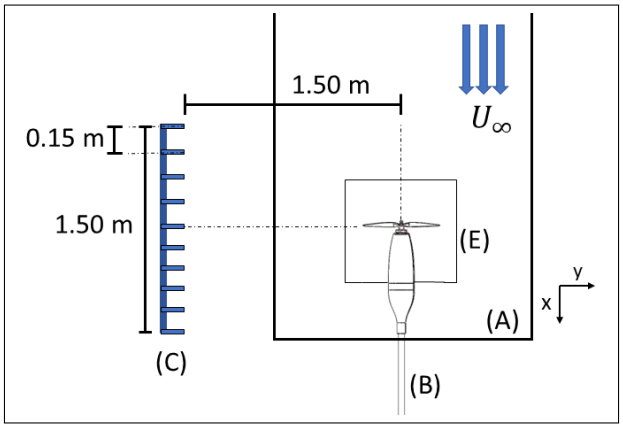

Figure 3. Linear array (top view). (A) Flat plate; (B) Propulsive system; (C) Linear array of microphones; (E) Quarter wave resonator elements.

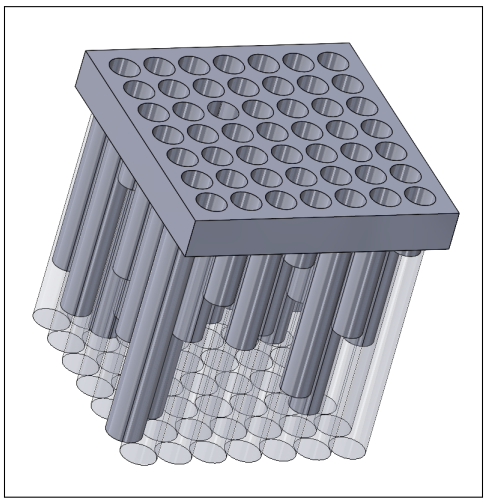

Figure 4. Noise absorption piece. The active face where the holes are is $0.1 \times 0.1m^2$. The piece was 3D printed by the FDM method. Detail shows the different tube lengths inside the piece.

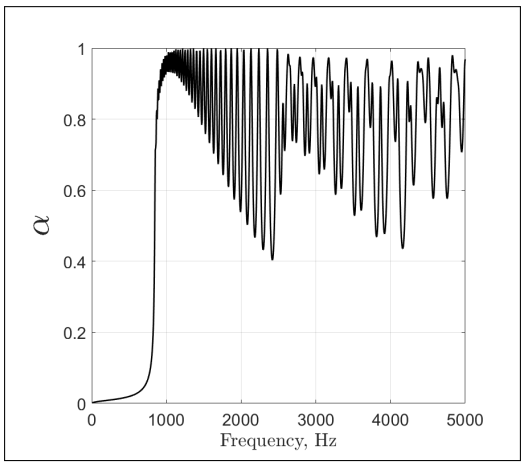

Figure 5. Coefficient of absorption of a single piece (N = 49, R = 0.0055 m, $\Omega = 0.465$). The frequency range between 800 Hz and 1400 Hz is the most absorbed by each piece. The frequencies after 2000 Hz show the harmonics of the absorbed frequencies.

and Vibration module (NI PXIe-1073 chassis). The sampling frequency is 51.2 kHz. A 30 seconds acquisition time for each measurement was used. The Power Spectral Density is calculated by using Welch's method for a frequency of 2^{16} Hz and a 50% window overlap, corresponding to an 8 Hz bandwidth size.

3.1 Noise absorber elements

The design of the noise absorber piece uses the low reduced frequency model as described in Section 2. The piece consists of a set of tubes connected to a surface. The specific lengths and radii of the tubes are designed so that the incoming sound waves in a frequency range are absorbed. By setting up a frequency range, the Low reduced frequency model can be used to determine which length each tube needs for a given radius. The porosity is related to the number of tubes attached to each piece.

With a number of tubes $N = 49$, radius of $5.5mm$ and an area of $0.1 \times 0.1m^2$ the porosity is $A_{tube}/A_{total} = 0.0095$. Figure 5 shows the absorption coefficient α as a function of frequency for each piece. Nine noise absorption pieces are positioned under the propeller in a $0.3 \times 0.3m^2$ slot and covered with a Kevlar cloth.The whole absorber setup (pieces + Kevlar) is flush with the flat plate. The Kevlar ensures that only the noise is absorbed and that the pieces do not influence the incoming flow. The measurements are conducted for the baseline configuration (propeller and flat plate) and noise mitigation configuration (propeller and noise absorbers).

4. RESULTS AND DISCUSSION

The effects of the noise absorption elements, for the case of the propeller condition of 6000 rpm rotation speed and 30 m/s flow speed, are investigated. This condition represents an advance ratio of 0.98 and an efficiency of 0.72, close to the maximum efficiency of the propeller, as shown in [10].

By changing the boundary layer thickness, the propeller will operate in a different loading condition due to the immersion ratio of the blades. Immersion ratio is defined as the ratio between the diameter of the propeller and the boundary layer thickness impinging on the propeller. This causes an unsteady load variation on the blade profiles, expected to lead to higher noise. The noise absorber underneath the propeller influences the noise reflection.

Figure 6 shows the measured noise of the propeller with two different boundary layer thicknesses. For the thicker boundary layer - Figure 6(b) there is an broadband noise reduction close to the frequencies of interest. That is a minor noise reduction - less than 2 dB, predominant at the frequencies the noise absorber is efficient. Therefore, one can infer that this reduction is real and not caused by

a measurement uncertainty.

The use of a broader bandwidth can help improve the noise analysis. The one-third-octave frequency band is a better way of visualising what happens around the frequencies of interest. Figure 7 shows the One-third-octave bandwidth distribution for each boundary layer thickness, where $\Delta SPL = SPL_{mitigation} - SPL_{flatplate}$ For the lower frequencies ($25Hz < f < 200Hz$), there is a reduction in most of the bins for the Trip 0 and Trip 2. Trip 1 shows an increase in noise on most of the centre frequencies. Low frequencies can be affected by mechanical and wind tunnel oscillations. That fact, and those varying results, show that for lower frequencies it is difficult to assess the effects of the noise absorber. In the range $200Hz < f < 1500$, there is an increase in noise. This region is where the high Blade Passing Frequency tones are . The quarter-wave tubes act as a resonant body and couple with the frequency-specific tones of the propeller. This noise increase is seen in all cases, and can even be observed in the SPL analysis. Finally, for the higher frequencies ($1500Hz < f < 5000Hz$), a small noise reduction is seen for the linear array. The noise reduction happens in all cases, being more evident for lower boundary layer thicknesses and less effective as the thickness increase.

When looking at the OASPL directivity in Figure 8, it is clear that the mitigation surface addition does not affect the directivity pattern. For advance ratios close to unity, the mitigation unit showed better efficiency in reducing overall noise for the thicker boundary layer case. That may be because, as analyzed previously, the noise absorber absorbs broadband noise. For the case of Trip 2 a large boundary layer is generated for the unsteady loading to be somewhat more uniform than for smaller boundary layer heights. The linear array also show the same behaviour (Figure 9). The directivity of the linear array for the baseline configuration is slightly different from the polar array. This results is expected as previously shown in [10].

Lastly, Figure 10 shows the propeller in a different condition: 5000 rpm, J = 1.13. In this condition, the efficiency is 0.65, below the one at J near unity. Here the better results are for Trip 1. At lower efficiency, boundary layer of the blades has more separation regions, which implies higher turbulence structures and a higher broadband noise. But because increasing the rotation speed also results in higher noise, this result means that the overall noise reduction increase doesn't follow a clear logic. A more thorough analysis of the effects of introducing noise mitigation shall be done to further understand the efficiency of the absorbing element used.

5. CONCLUSIONS

This research shows an experimental analysis of a noise mitigation technique for the surface under boundary layer ingesting propellers. A set of quarter-wave resonators is designed using the low reduced frequency model for coupled tubes. The mitigation surfaces are positioned on a flat plate under the propeller so there is broadband absorption at frequencies in the range of $800Hz < f < 2000Hz$. The results show the efficiency of the mitigation method at frequencies close to the region of interest. However, the tonal characteristics of the propeller noise are intensified by the presence of the absorber. Also, the overall noise directivity results show that the benefit of the absorber does not follow a clear logic with the constraints changed in the experiments. Those effects might have been caused by the presence of the Kevlar on top of the mitigation unit. The Kevlar is not rigid and probably was under a vibration phenomenon when under the flow, resonating with the blade passing frequencies of the propeller. Also, its porosity might have changed the effective frequency absorbed by the pieces.

Following this preliminary analysis of passive surface noise mitigation for BLI propellers. In future work, the analysis of different methods of passive mitigation (liners, acoustic black holes, other complex resonators) shall be investigated. The effects of the Kevlar on top of the mitigation unit has to be investigated to confirm any coupling with the rotation of the propeller blades. Also, more cases should be analyzed, as for the propeller at low advance ratios (take-off). An absorber with a narrow frequency band can also be tested to check its ability to mitigate tonal noise.

6. ACKNOWLEDGMENTS

This research is supported by the European Union's Horizon 2020 project ENODISE (860103). The authors would like to thank the University of Twente technical staff, Ing. W. Lette, S. Wanrooij, and E. Leusink, for the extensive help on the experimental setup.

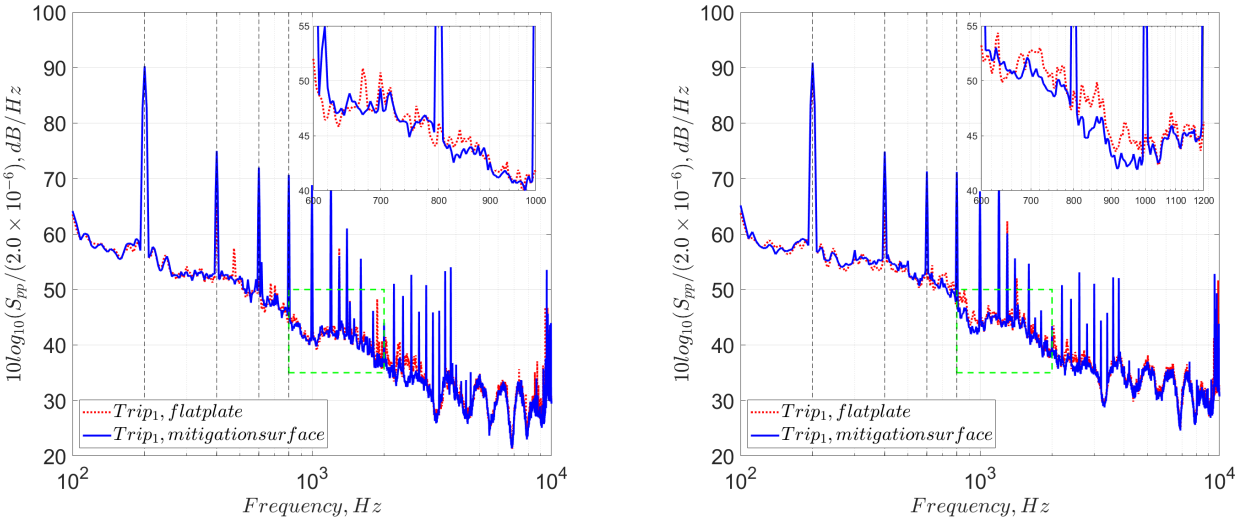

(a) Trip 0 ($\delta/D = 0.18$) (b) Trip 2 ($\delta/D = 0.45$)

Figure 6. Noise characteristics of propeller for two different boundary layer heights (90°microphone, polar array). In detail, a zoom of the graph, highlighting the frequencies of interest. The vertical dashed lines show the blade passing frequencies.

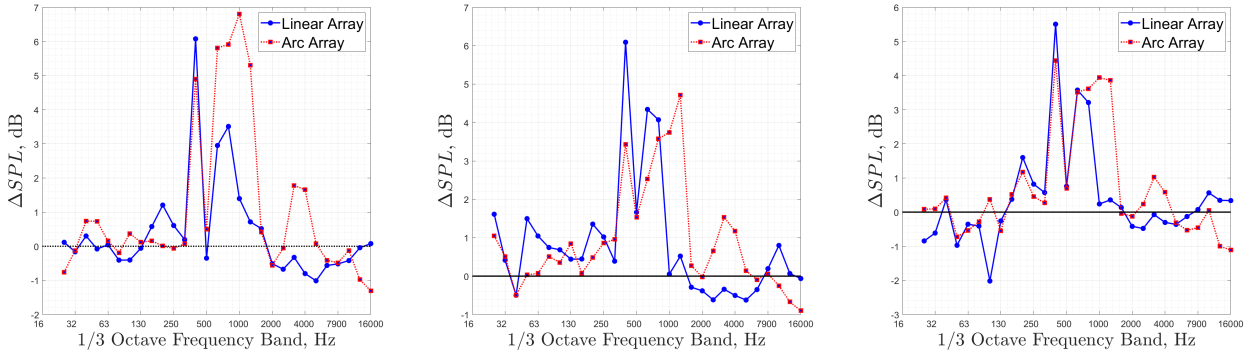

(a) Trip 0 ($\delta/D = 0.18$) (b) Trip 1 ($\delta/D = 0.34$) (c) Trip 2 ($\delta/D = 0.45$)

Figure 7. One-third-octave frequency band showing the effect of increasing the boundary layer (90°microphone).

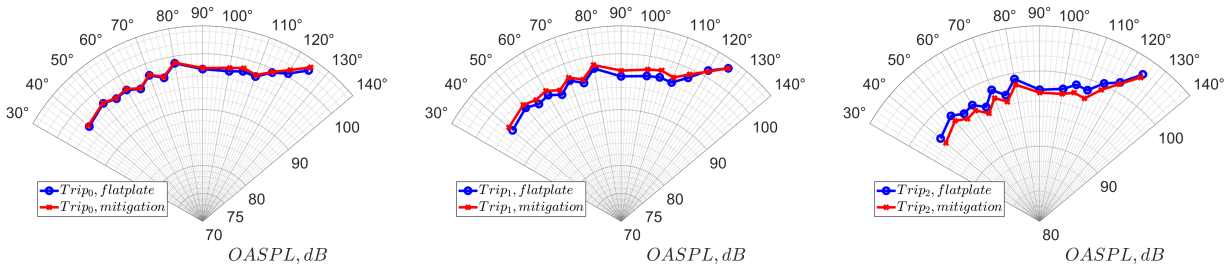

(a) Trip 0 ($\delta/D = 0.18$) (b) Trip 1 ($\delta/D = 0.34$) (c) Trip 2 ($\delta/D = 0.45$)

Figure 8. Polar directivity, arc array (J = 0.98, 6000 rpm).

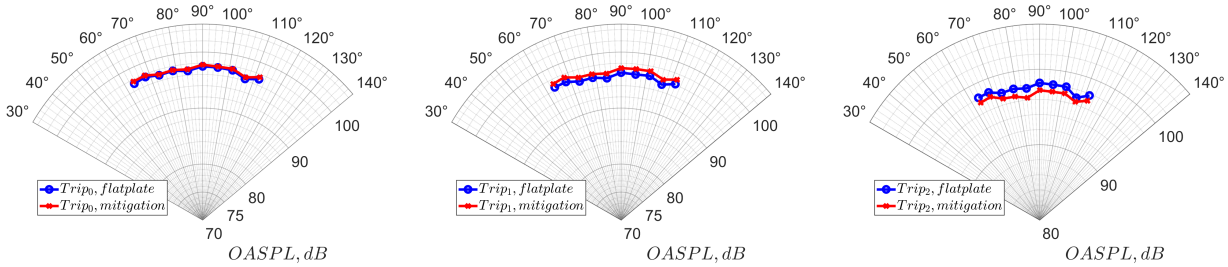

(a) Trip 0 ($\delta/D = 0.18$) (b) Trip 1 ($\delta/D = 0.34$) (c) Trip 2 ($\delta/D = 0.45$)

Figure 9. Polar directivity, linear array (J = 0.98, 6000 rpm).

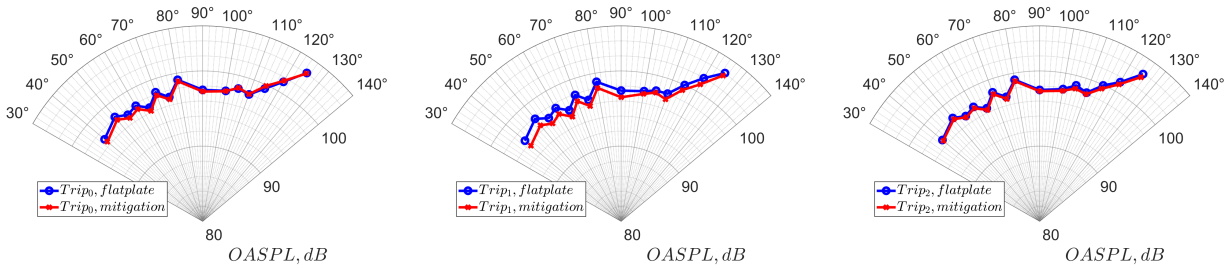

(a) Trip 0 ($\delta/D = 0.18$) (b) Trip 1 ($\delta/D = 0.34$) (c) Trip 2 ($\delta/D = 0.45$)

Figure 10. Polar directivity, arc array (J = 1.13, 5000 rpm)

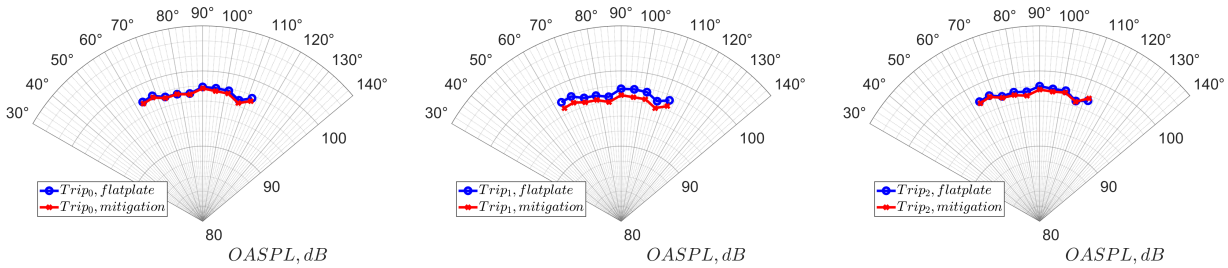

(a) Trip 0 ($\delta/D = 0.18$) (b) Trip 1 ($\delta/D = 0.34$) (c) Trip 2 ($\delta/D = 0.45$)

Figure 11. Polar directivity, linear array (J = 1.13, 5000 rpm).

7. REFERENCES

[1] S. A. Rizzi, D. L. Huff, D. D. Boyd, P. Bent, B. S. Henderson, K. A. Pascioni, D. C. Sargent, D. L. Josephson, M. Marsan, H. B. He, *et al.*, "Urban air mobility noise: Current practice, gaps, and recommendations," tech. rep., 2020.

[2] J. Xie, L. Zhu, and H. M. Lee, "Aircraft noise reduction strategies and analysis of the effects," *International Journal of Environmental Research and Public Health*, vol. 20, no. 2, p. 1352, 2023.

[3] M. A. S. Abdul Kaiyoom, A. Yildirim, and J. R. Martins, "Coupled aeropropulsive design optimization of an over-wing nacelle configuration," in *AIAA SCITECH 2023 Forum*, p. 0327, 2023.

[4] D. Ingraham, J. S. Gray, and L. V. Lopes, "Gradient-based propeller optimization with acoustic constraints," in *Aiaa scitech 2019 forum*, p. 1219, 2019.

[5] S. T. Go, M. J. Kingan, R. S. McKay, and R. N. Sharma, "Theoretical investigation of the turbulent inflow noise produced by a shrouded propeller," in *28th AIAA/CEAS Aeroacoustics 2022 Conference*, p. 2831, 2022.

[6] F. J. M. van der Eerden, *Noise reduction with coupled prismatic tubes*. Universiteit Twente, Enschede, The Netherlands, 2000.

[7] L. D. de Santana, M. P. Sanders, C. H. Venner, and H. W. Hoeijmakers, "The utwente aeroacoustic wind tunnel upgrade," in *2018 AIAA/CEAS Aeroacoustics Conference*, p. 3136, 2018.

[8] "Development of computational and experimental noise assessment and suppression methodologies for the next generation of silent distributed propulsion configurations," 2020. Last accessed 30 May 2022.

[9] A. Silvestri, F. Ghanadi, M. Arjomandi, B. Cazzolato, and A. Zander, "The application of different tripping techniques to determine the characteristics of the turbulent boundary layer over a flat plate," *Journal of Fluids Engineering, Transactions of the ASME*, vol. 140, pp. 1–12, 2018. boundarylayerthickness¡br/¿boundarylayer.

[10] L. A. Castelucci, C. H. Venner, and L. D. de Santana, "Experimental analysis of the noise of small propellers subjected to non-uniform inflow," in *AIAA SCITECH 2023 Forum*, p. 1545, 2023.

[11] S. Guérin, T. Lade, L. Castelucci, and I. Zaman, "Tonal noise emission by a low-mach low-reynolds number propeller ingesting a boundary layer," 2023.